nature climate change

LETTERS

https://doi.org/10.1038/s41558-018-0244-4

Seasonally dependent responses of subtropical highs and tropical rainfall to anthropogenic warming

Fengfei Song*, L. Ruby Leung*, Jian Lu and Lu Dong

The subtropical highs are semi-permanent atmospheric features that strengthen during April–September, exerting a large influence on regional rainfall[1–5]. Previous studies have focused on the changes of subtropical highs during their peak season (June–August)[6–8], but little is known about their changes in other seasons. Here, a suite of multi-model simulations are used to demonstrate the robust seasonally dependent responses of subtropical highs and tropical rainfall to anthropogenic warming. The zonal-mean subtropical highs in the Northern Hemisphere are shown to strengthen more during April–June than July–September, with opposite responses for the Southern Hemisphere counterparts. These responses are closely related to a southward shift of tropical rainfall in April–June relative to July–September, manifesting in a seasonal delay of tropical rainfall and monsoon onset in the Northern Hemisphere[9,10]. Such seasonality is found to occur in response to elevated latent energy demand in the hemisphere warming up seasonally, as dictated by the Clausius–Clapeyron relation. The interhemispheric energy contrast drives a southward shift of tropical rainfall that strengthens the Hadley cell and zonal-mean subtropical highs in the Northern Hemisphere in April–June relative to July–September. These changes scale linearly with warming, with increasing implications for projecting climate changes in the tropics and subtropics as warming continues.

The subtropical highs can be viewed as the combined contribution from the descending branch of the Hadley cell and the zonally asymmetric diabatic heating associated with land/sea distribution, with their relative contributions varying significantly with season[11–13]. In the Northern Hemisphere, they are most evident over the subtropical oceans, and known as the North Pacific subtropical high and North Atlantic subtropical high. The Southern Hemisphere counterpart is more zonally distributed. During April–September, the North Pacific subtropical high and the North Atlantic subtropical high strengthen and exert substantial influences on precipitation over East Asia and North America, home to more than two billion people, by modulating the moisture transport[1,2] and tropical cyclone tracks[3–5] directed to the regions. Meanwhile, the Southern Hemisphere subtropical high also strengthens, and the associated trade winds transport substantial moisture to the Northern Hemispheric monsoon regions, including the Sahel, South Asia, East Asia and North America[2,14,15].

Previous studies suggest that under global warming, the North Atlantic subtropical high will intensify and move westward during June–August[6,7], but changes in the North Pacific subtropical high are more uncertain[6–8]. Few studies have paid attention to seasons other than June–August, even though the subtropical highs are also well defined and substantively strong during April–June (Supplementary Fig. 1). Even less well studied is how the Southern Hemisphere subtropical high will change under global warming[16]. Here, we find that changes of the zonal-mean subtropical high under global warming have marked seasonal dependence, which is related to the tropical precipitation delay[9,10]. These seasonally dependent changes originate from the climatological seasonal cycle of temperature through the constraint of the Clausius–Clapeyron relation. These results have important implications for projecting changes in the global hydrological cycle and atmospheric circulations of the tropics and subtropics.

Here, the historical (HIST) and Representative Concentration Pathway 8.5 (RCP8.5) simulations from 37 Coupled Model Intercomparison Project phase 5 (CMIP5; ref. [17]; see Methods) models are used to represent the current and future climates, respectively. Figure 1a,b shows that the present-day subtropical highs in April, May and June (AMJ) and July, August and September (JAS) are comparable in magnitude. In the future warming scenario (Fig. 1c), the zonal-mean subtropical high in the Northern Hemisphere does not show robust changes during either AMJ or JAS, but there is an evident strengthening of the zonal-mean subtropical high in AMJ relative to JAS. More specifically, 35 out of the 37 models show more strengthening during AMJ than JAS for the zonal-mean subtropical high (Supplementary Fig. 2). This seasonal dependence also occurs in the Southern Hemispheric counterpart, with stronger enhancement during JAS than AMJ instead (34 out of 37 models). The mid-latitude westerly at the poleward flank of the subtropical high shows the consistent changes in both hemispheres (Fig. 1c and Supplementary Fig. 2). We focus on the zonal-mean subtropical highs because the inter-seasonal difference in the response of the zonally asymmetric subtropical highs is insignificant (Supplementary Fig. 3).

Tropical precipitation change also exhibits a clear seasonal dependence under global warming (Fig. 2), which will be demonstrated to be responsible for the zonal-mean subtropical high response. Broadly, the precipitation response is characterized by the 'wet-get-wetter'[18,19] and 'warmer-get-wetter'[20,21] patterns, with the former representing an enhancement of the climatological seasonal cycle pattern due to the increase of moisture with warming, and the latter manifesting as a larger precipitation increase at the equatorward flank of the climatological rainband following the accentuated equatorial sea surface temperature (SST) warming[22] (Fig. 2a,b,d,e). Closer inspection reveals evident deviations of the

Atmospheric Sciences and Global Change Division, Pacific Northwest National Laboratory, Richland, WA, USA. *e-mail: Fengfei.Song@pnnl.gov; Ruby.Leung@pnnl.gov

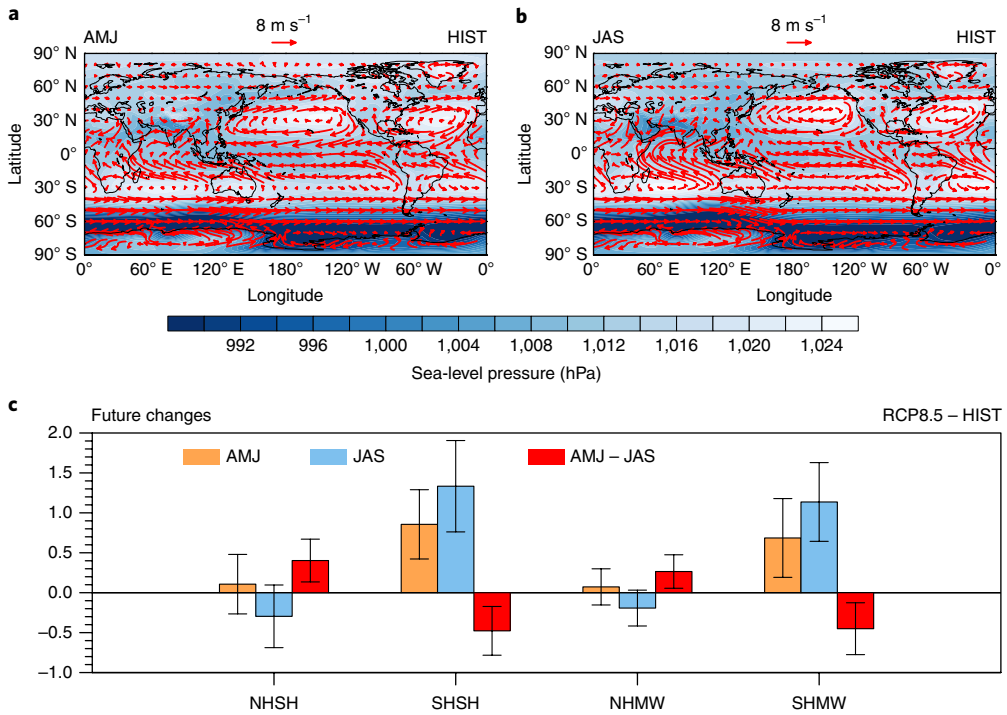

Fig. 1 | Seasonal dependence of the changes in the zonal-mean subtropical highs under global warming. a,**b**, Climatology of the 925 hPa wind (arrows) and sea-level pressure (shading) in the HIST experiment during AMJ (**a**) and JAS (**b**). **c**, Future changes between RCP8.5 and HIST during AMJ (orange), JAS (blue) and AMJ minus JAS (red). Left to right: Northern Hemispheric subtropical high (NHSH; 25°–45° N; unit: hPa), Southern Hemispheric subtropical high (SHSH; 20°–40° S; unit: hPa), Northern Hemispheric mid-latitude westerly (NHMW; 40°–55° N; unit: m s^{-1}) and Southern Hemispheric mid-latitude westerly (SHMW; 40°–55° N; unit: m s^{-1}). The error bars show one standard deviation among models.

tropical precipitation change from the climatological seasonal cycle (Fig. 2d,e) and a conspicuous dipole change straddling the climatological peak during June–August at about 10° N (Fig. 2a,b), signalling a delay in the arrival of monsoonal rainfall[9,10]. Removal of the wet-get-wetter and warmer-get-wetter components (see Methods) amplifies the suppression of precipitation in the early warm season in both hemispheres during their respective transition from spring to summer (Fig. 2c,f).

Figure 3 depicts the seasonal differences in the zonal-mean precipitation and circulation changes between AMJ and JAS. In response to the RCP8.5 forcing, the subtropical high pressure exhibits a robust inter-seasonal increase in the Northern Hemisphere and a decrease in the Southern Hemisphere (Fig. 3a). Meanwhile, the inter-seasonal difference of tropical precipitation change is characterized by a dipole pattern, with negative and positive changes north and south of the Equator, respectively. Changes in the position of tropical precipitation and the associated peak heating have a profound asymmetric influence on the strength of the Hadley cell in both hemispheres. The inter-seasonal dipolar precipitation anomaly (Fig. 3a) is expected to enhance the Northern Hemispheric Hadley cell and weaken the Southern Hemispheric counterpart, according to Hadley cell theory under interhemispherically asymmetric forcing[23]. This is confirmed by the alternating bands of vertical velocity response in Fig. 3e (with positive denoting ascent), showing an enhanced/weakened descent near 35° N/35° S (see also Supplementary Fig. 4 for the stream function response) in AMJ relative to JAS under warming. Consistent with the southward shift of the tropical precipitation, the centre of the Hadley cell shifts southward in almost all models during AMJ relative to JAS. Coinciding with the anomalous descent and ascent of the Hadley cell response, the zonal-mean subtropical high intensifies in the Northern Hemisphere and weakens in the Southern Hemisphere (Fig. 3a).

To understand the physical processes of the seasonally dependent changes, the climate response can be decomposed into components associated with direct radiative CO_2 forcing and indirect SST warming[7]. We use Atmospheric Model Intercomparison Project (AMIP) experiments in which SST is prescribed (see Methods) to estimate the two components. The component associated with direct radiative forcing can be approximated by quadrupling the CO_2 concentration without SST changes (AMIP4×CO_2), while the component associated with the indirect SST warming can be estimated by adding an SST warming pattern derived from the coupled atmosphere/ocean model response to increased CO_2 (AMIPFuture) or increasing SST uniformly by 4 K (AMIP4K). The combined responses of atmospheric circulation and tropical precipitation to direct radiative forcing and indirect SST warming resemble the response under the RCP8.5 scenario in the zonal-mean sense (Supplementary Figs. 5 and 6).

Under the direct radiative forcing (Fig. 3b,f), seasonal differences in the changes of the zonal-mean subtropical highs in both hemispheres are generally weak and do not match the RCP8.5 responses. In contrast, both experiments with the SST warming pattern (Fig. 3c,g) and uniform SST warming (Fig. 3d,h) reproduce qualitatively the seasonally dependent responses of RCP8.5 (Fig. 3a,e). The seasonal delay of tropical precipitation is also reproduced well under the SST warming pattern, but not in the direct radiative forcing (Supplementary Figs. 7 and 8). Consistent with the anomalies of tropical precipitation, both of the SST warming experiments also reproduce the strengthening and weakening of the Hadley cell in the Northern Hemisphere and Southern Hemisphere, respectively, in AMJ compared with JAS (Supplementary Fig. 4). Hence, the seasonally dependent responses in the zonal-mean subtropical highs and the tropical precipitation seasonal delay can be attributed to SST warming.

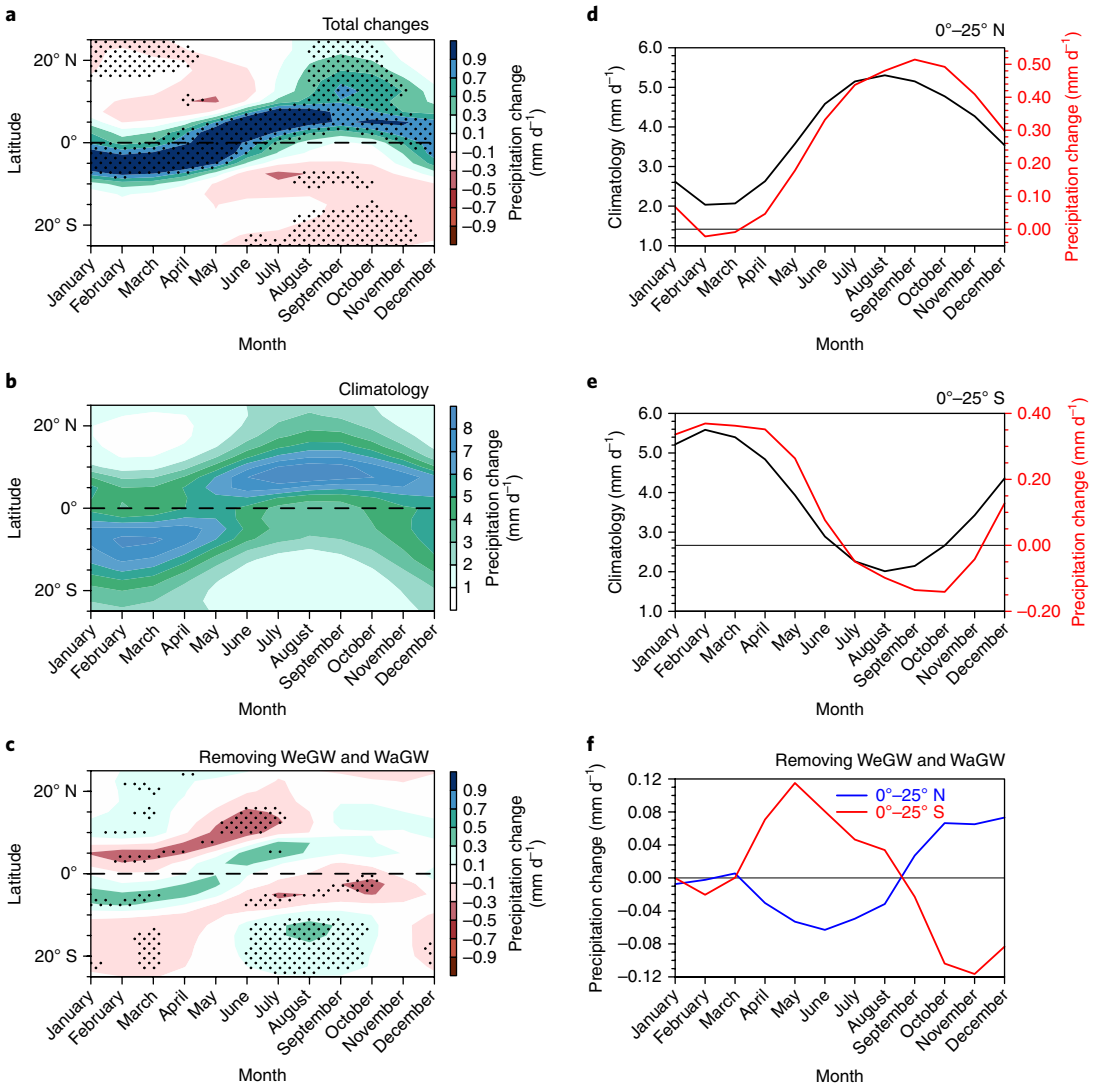

Fig. 2 | The seasonal delay of tropical precipitation under global warming. a, Precipitation change between the RCP8.5 and HIST runs. **b**, Climatology of tropical precipitation in the HIST run. **c**, Same as **a** but with the wet-get-wetter (WeGW) and warmer-get-wetter (WaGW) patterns removed. **d**,**e**, Climatology (black line) and change (red line) in the precipitation averaged over the northern tropics (0°–25° N) (**d**) and the southern tropics (0°–25° S) (**e**). **f**, Precipitation changes in the northern and southern tropics after removing the WeGW and WaGW. Stippling in **a** and **c** indicates that at least 70% of the models agree on the sign of the difference.

Recent advances[24–26] in understanding the shift of tropical precipitation from an energetics perspective provide a framework for explaining how SST warming causes a seasonally dependent atmospheric response globally. In the energetics framework[24–26], a southward displacement of tropical precipitation corresponds to a northward cross-equatorial atmospheric energy transport anomaly, and vice versa. This relation is dictated by the atmospheric structure in the tropics: the direction of atmospheric energy transport is determined by the upper branch of the Hadley cell as the moist static energy is higher in the upper level than the lower level, while the interhemispheric moisture transport is in an opposite direction, dominated by the lower branch of the Hadley cell.

The atmospheric energy transport is determined by the difference between the net input energy, F_{net}, and the tendency of the moist static energy, $\frac{\partial < h >}{\partial t}$ (equation (2), in Methods), where $< >$ represents the vertical integration between the surface and the top of the model, $F_{net}=F_{SFC}+F_{TOA}$,F_{SFC} is the net heat flux entering the atmosphere from the surface, F_{TOA} is the net radiation at the top of the atmosphere, t is time, $h=c_pT+gz+L_vq$ is the moist static energy, c_p is specific heat at constant pressure, T is air temperature, g is acceleration due to gravity, z is the geopotential height, L_v is latent heat of vaporization and q is specific humidity. With the uniform SST warming or SST warming pattern, the seasonal difference in the change of F_{net} between AMJ and JAS has strong meridional variations, but small interhemispheric contrast (Fig. 4a). However, the seasonal difference in the change of the negative moist static energy tendency, $-\frac{\partial < h >}{\partial t}$, shows a strong interhemispheric contrast, with the Southern Hemisphere 1.74 W m^{-2} and 2.16 W m^{-2} higher than the Northern Hemisphere in the uniform SST warming and SST warming pattern, respectively (Fig. 4b). Further decomposing h suggests that the seasonal difference in the change of the negative latent energy tendency, $-\frac{\partial < L_vq >}{\partial t}$ (Fig. 4c), accounts for most of the interhemispheric contrast shown in Fig. 4b. The interhemispheric energy contrast requires a northward cross-equatorial energy transport for energy balance (Fig. 4d), which is 0.42 PW and 0.24 PW in the SST warming pattern and uniform SST warming cases, respectively. The difference of cross-equatorial energy transport between the SST warming pattern and uniform SST warming suggests that the seasonal difference of SST change pattern (Supplementary Fig. 9) is also

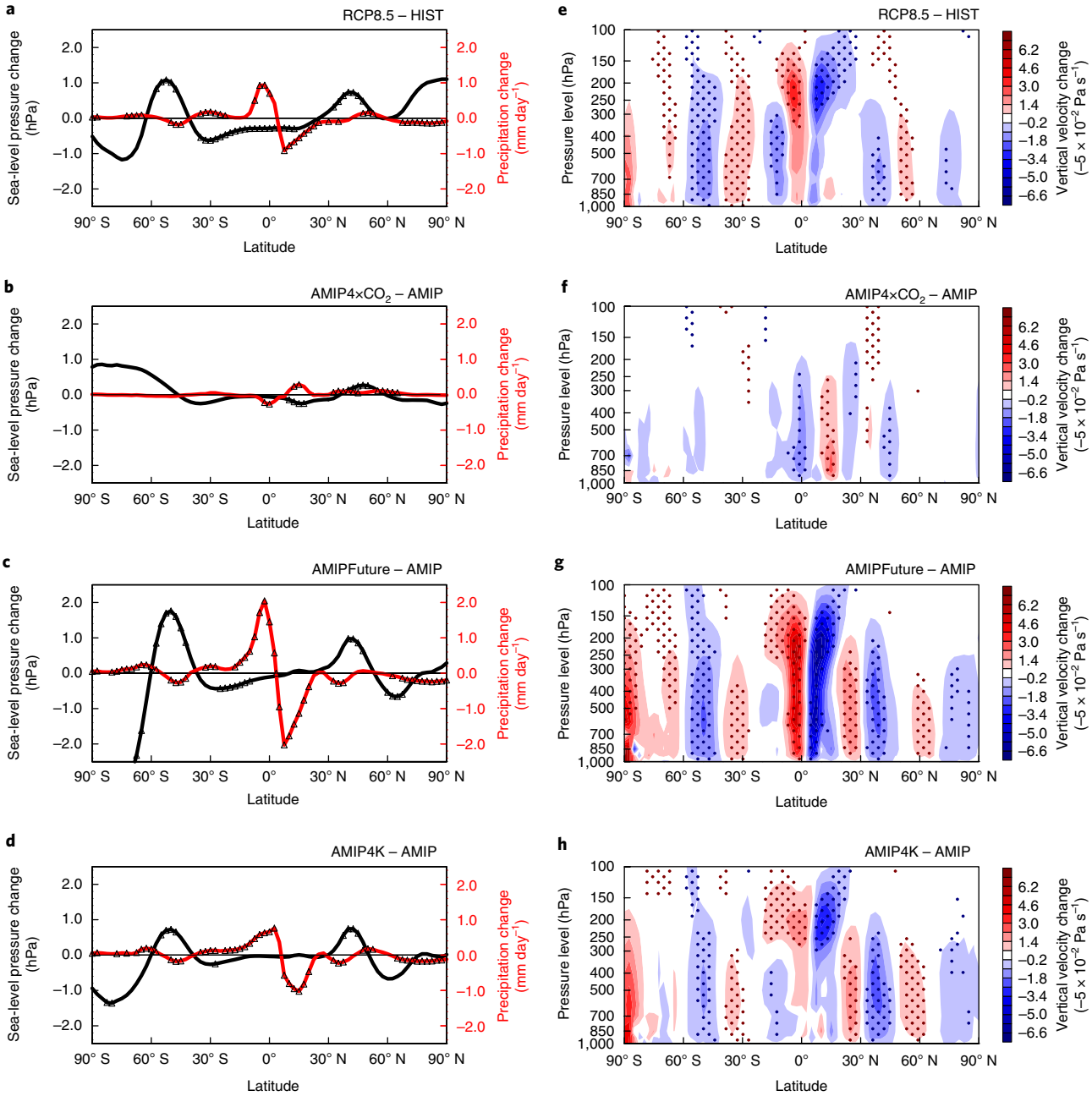

Fig. 3 | The difference of zonal-mean precipitation and atmospheric circulation changes between AMJ and JAS under global warming. a–d, Sea-level pressure (black) and precipitation (red) changes under RCP8.5 (**a**), direct radiative forcing (**b**), SST warming pattern (**c**) and uniform SST warming (**d**). **e–h**, Same as the corresponding panels **a–d** but for the vertical velocity changes, with positive values denoting ascent. The triangles in **a–d** and stippling in **e–h** indicate that at least 70% of the models agree on the sign of the difference.

important for tropical precipitation delay[9]. The cross-equatorial energy transport is dominated by the moist static energy tendency. Among the moist static energy tendency, the contribution from latent energy tendency accounts for 70% and 85% under the SST warming pattern and uniform SST warming, respectively (Fig. 4d). The coupled models show similar results (Supplementary Fig. 10). The northward cross-equatorial energy transport corresponds well to the southward shift of tropical precipitation, with inter-model correlation coefficients of −0.4, −0.61 and −0.66 for RCP8.5, AMIPFuture and AMIP4K, respectively, all statistically significant at a 99% confidence level. The northward cross-equatorial energy transport due to the moist static energy tendency also corresponds well to the change of subtropical highs in both hemispheres (Supplementary Fig. 11), with inter-model correlation coefficients of 0.58 and −0.47 for the zonal-mean subtropical highs in the Northern Hemisphere and Southern Hemisphere, respectively.

On the basis of the Clausius–Clapeyron relation, the change in the latent energy tendency, $\Delta\frac{\partial<L_vq>}{\partial t}$, under global warming is proportional to the climatological temperature tendency, $\frac{\partial T_s}{\partial t}$ (see the derivation in Methods):

$$\Delta\frac{\partial<L_vq>}{\partial t}\approx a\Delta T_s\frac{\partial T_s}{\partial t} \quad (1)$$

where a is a parameter determined by the present climate state and ΔT_s is the surface temperature change. Because both a and

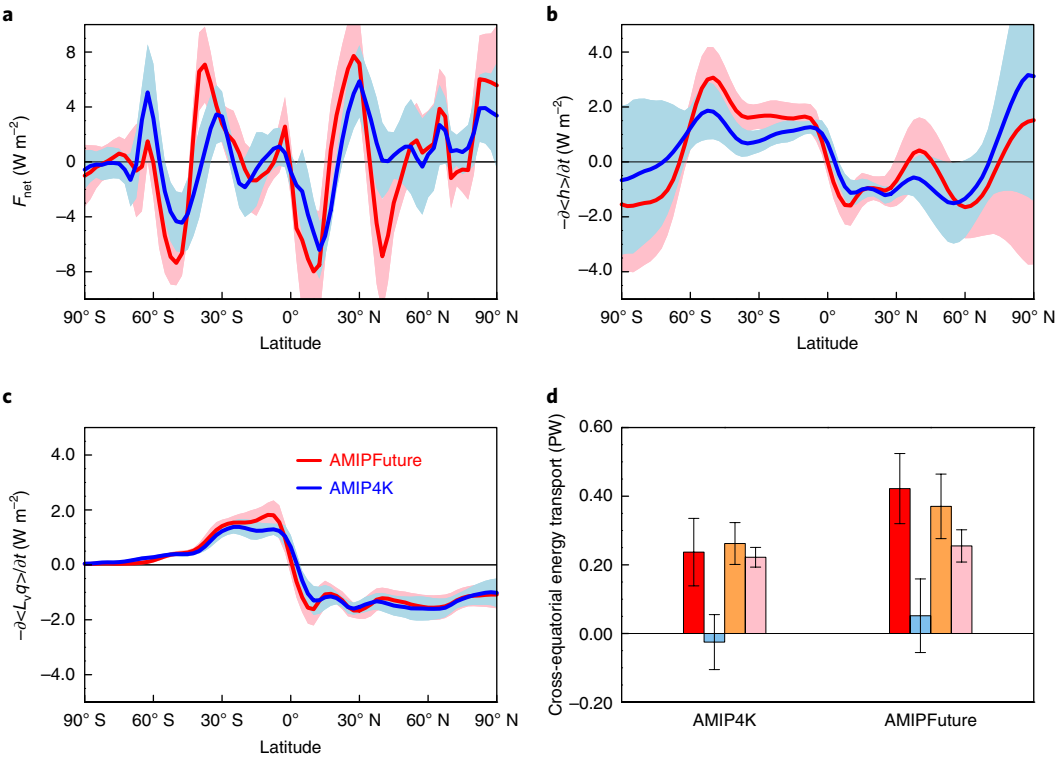

Fig. 4 | The difference in atmospheric energy change between AMJ and JAS under the indirect SST warming. a–**c**, Net atmospheric energy flux, F_{net} (**a**), vertically integrated negative atmospheric energy tendency, $-\frac{\partial < h >}{\partial t}$ (**b**) and vertically integrated negative latent energy tendency, $-\frac{\partial < L_vq >}{\partial t}$ (**c**) for changes between AMIP4K (blue line) or AMIPFuture (red line) and AMIP. The pink and blue ribbons represent one standard deviation among models for AMIP4K and AMIPFuture changes, respectively. **d**, The cross-equatorial energy transport change (red) and its contributions from F_{net} (blue), $-\frac{\partial < h >}{\partial t}$ (orange) and $-\frac{\partial < L_vq >}{\partial t}$ (pink) between AMIP4K or AMIPFuture and AMIP experiments. The error bars in **d** represent one standard deviation among models.

ΔT_s have weak seasonal variations, the seasonal cycle of $\Delta\frac{\partial < L_vq >}{\partial t}$ is dominated by $\frac{\partial T_s}{\partial t}$, with correlation coefficients of nearly 0.90 or higher. From equation (1), it is easy to see why $\Delta\frac{\partial < L_vq >}{\partial t}$ has a striking interhemispheric contrast between AMJ and JAS: during AMJ, the Northern Hemisphere is rapidly warming up ($\frac{\partial T_s}{\partial t} > 0$) and the Southern Hemisphere is cooling down ($\frac{\partial T_s}{\partial t} < 0$), whereas JAS is the warmest and coldest season in the Northern Hemisphere and Southern Hemisphere, respectively, with weak temperature tendency ($\frac{\partial T_s}{\partial t} \approx 0$; Supplementary Fig. 12). In a warmer world (positive ΔT_s), more latent energy is needed to warm up the Northern Hemisphere, and more latent energy must be removed from the Southern Hemisphere for it to cool down during AMJ, according to equation (1). To keep up with the moist static energy tendency, the atmosphere must transport more energy from the Southern Hemisphere to the Northern Hemisphere. Thus, the Hadley cell and tropical precipitation shift southward during AMJ relative to JAS. This anomalous energy transport originated from the climatological seasonal cycle of temperature is also evident, but in the opposite direction, during October–December (Supplementary Fig. 13), when the Northern Hemisphere is cooling down and the Southern Hemisphere is warming up.

In summary, the climatological seasonal cycle of temperature dictates that under global warming, the transitional season (April–June and October–December) engenders larger cross-equatorial energy transport to the hemisphere that is warming up seasonally, due to the latent energy tendency change, as required by the Clausius–Clapeyron relation. Under this energy constraint, tropical precipitation shifts to the hemisphere that is cooling down seasonally, hence resulting in a seasonal delay in the migration of tropical precipitation from the cold hemisphere to the warm hemisphere. Relative to JAS, the southward shift of the tropical precipitation during AMJ strengthens the Hadley cell in the Northern Hemisphere and weakens it in the Southern Hemisphere. As an integral part of the descending branch of the Hadley cell, the zonal-mean subtropical high in the Northern Hemisphere is intensified, while the counterpart in the Southern Hemisphere is weakened, in AMJ relative to JAS (see the schematic plot of Supplementary Fig. 14).

Because the change in the latent energy tendency scales linearly with global warming from equation (1), it is expected that the seasonally dependent responses of the zonal-mean subtropical highs and tropical precipitation seasonal delay will become more evident as global warming continues. This has increasing implications for projecting future changes in the tropics and subtropics. This study focuses only on the zonal-mean aspect of the inter-seasonal response for which the mechanism we have proposed applies. Zonally asymmetric factors such as land/sea contrast are also important for the subtropical circulation, so their relative roles in the total subtropical high response to warming at a more regional scale warrant further investigation in the future.

Methods

Methods, including statements of data availability and any associated accession codes and references, are available at https://doi.org/10.1038/s41558-018-0244-4.

Received: 2 January 2018; Accepted: 6 July 2018;
Published online: 06 August 2018

References

1. Li, W., Li, L., Fu, R., Deng, Y. & Wang, H. Changes to the North Atlantic subtropical high and its role in the intensification of summer rainfall variability in the southeastern United States. *J. Clim.* **24**, 1499–1506 (2011).

2. Zhou, T. & Yu, R. Atmospheric water vapor transport associated with typical anomalous summer rainfall patterns in China. *J. Geophys. Res.* **110**, D08104 (2005).
3. Colbert, A. & Soden, B. Climatological variations in North Atlantic tropical cyclone tracks. *J. Clim.* **25**, 657–673 (2012).
4. Stowasser, M., Wang, Y. & Hamilton, K. Tropical cyclone changes in the western North Pacific in a global warming scenario. *J. Clim.* **20**, 2378–2396 (2007).
5. Wu, L., Wang, B. & Geng, S. Growing typhoon influence on East Asia. *Geophys. Res. Lett.* **32**, L18703 (2005).
6. Li, W., Li, L., Ting, M. & Liu, Y. Intensification of Northern Hemisphere subtropical highs in a warming climate. *Nat. Geosci.* **5**, 830–834 (2012).
7. Shaw, T. A. & Voigt, A. Tug of war on the summertime circulation between radiative forcing and sea surface warming. *Nat. Geosci.* **8**, 560–566 (2015).
8. He, C., Wu, B., Zou, L. & Zhou, T. Responses of the summertime subtropical anticyclone to global warming. *J. Clim.* **30**, 6465–6479 (2017).
9. Biasutti, M. & Sobel, A. H. Delayed Sahel rainfall and global seasonal cycle in a warmer climate. *Geophys. Res. Lett.* **36**, L23707 (2009).
10. Dwyer, J. G., Biasutti, M. & Sobel, A. H. The effects of greenhouse gas-induced changes in SST on the annual cycle of zonal mean tropical precipitation. *J. Clim.* **27**, 4545–4565 (2014).
11. Namias, J. Influence of Northern Hemisphere general circulation on drought in northeast Brazil. *Tellus* **24**, 336–343 (1972).
12. Hoskins, B. J. On the existence and intensity of summer subtropical anticyclones. *Bull. Am. Meteorol. Soc.* **77**, 1287–1291 (1996).
13. Rodwell, M. J. & Hoskins, B. J. Subtropical anticyclones and summer monsoon. *J. Clim.* **14**, 3192–3211 (2001).
14. Wang, B. et al. Northern Hemisphere summer monsoon intensified by mega-El Niño/southern oscillation and Atlantic multidecadal oscillation. *Proc. Natl Acad. Sci. USA* **110**, 5347–5352 (2013).
15. Pathak, A., Ghosh, S., Martinez, J. A., Dominguez, F. & Kumar, P. Role of oceanic and land moisture sources and transport in the seasonal and interannual variability of summer monsoon in India. *J. Clim.* **30**, 1839–1859 (2017).
16. Li, W. et al. Intensification of the Southern Hemisphere summertime subtropical anticyclones in a warming climate. *Geophys. Res. Lett.* **40**, 5959–5964 (2013).
17. Taylor, K. E., Stouffer, R. J. & Meehl, G. A. An overview of CMIP5 and the experiment design. *Bull. Am. Meteorol. Soc.* **93**, 485–498 (2012).
18. Held, I. M. & Soden, B. J. Robust responses of the hydrological cycle to global warming. *J. Clim.* **19**, 5686–5699 (2006).
19. Chou, C., Neelin, J., Chen, C. & Tu, J. Evaluating the 'rich-get-richer' mechanism in tropical precipitation change under global warming. *J. Clim.* **22**, 1982–2005 (2009).
20. Xie, S.-P. et al. Global warming pattern formation: sea surface temperature and rainfall. *J. Clim.* **23**, 966–986 (2010).
21. Johnson, N. C. & Xie, S.-P. Changes in the sea surface temperature threshold for tropical convection. *Nat. Geosci.* **3**, 842–845 (2010).
22. Huang, P., Xie, S. P., Hu, K. M., Huang, G. & Huang, R. H. Patterns of the seasonal response of tropical rainfall to global warming. *Nat. Geosci.* **6**, 357–361 (2013).
23. Lindzen, R. S. & Hou, A. Y. Hadley circulations for zonally averaged heating centered off the Equator. *J. Atmos. Sci.* **45**, 2417–2427 (1988).
24. Kang, S. M., Held, I. M., Frierson, D. & Zhao, M. The response of the ITCZ to extratropical thermal forcing: idealized slab-ocean experiments with a GCM. *J. Clim.* **21**, 3521–3532 (2008).
25. Kang, S. M., Frierson, D. & Held, I. M. The tropical response to extratropical thermal forcing in an idealized GCM: the importance of radiative feedbacks and convective parameterization. *J. Atmos. Sci.* **66**, 2812–2827 (2009).
26. Schneider, T., Bischoff, T. & Haug, G. H. Migrations and dynamics of the intertropical convergence zone. *Nature* **513**, 45–53 (2014).

Acknowledgements

This research is supported by the US Department of Energy Office of Science Biological and Environmental Research as part of the Regional and Global Climate Modeling Program. This work has benefited from discussions with Z. Feng, R. A. Houze Jr, C. He and W. Zhou. PNNL is operated for the Department of Energy by Battelle Memorial Institute under contract DE-AC05-76RL01830. We acknowledge the World Climate Research Program's Working Group on Coupled Modeling, which is responsible for CMIP, and thank the climate modelling groups (listed in Supplementary Table 1) for producing and making available their model output. For CMIP, the US DOE's Program for Climate Model Diagnosis and Intercomparison (PCMDI) provides coordinating support and led the development of software infrastructure in partnership with the Global Organization for Earth System Science Portals.

Author contributions

L.R.L. and F.S. designed the research. F.S. performed the analysis alongside discussions with all other authors. F.S. and L.D. performed the theoretical derivation. J.L. contributed to improving the analysis and interpretation. F.S. wrote the first draft of this paper. All authors discussed and commented on the paper.

Competing interests

The authors declare no competing interests.

Additional information

Supplementary information is available for this paper at https://doi.org/10.1038/s41558-018-0244-4.

Reprints and permissions information is available at www.nature.com/reprints.

Correspondence and requests for materials should be addressed to F.S. or L.R.L.

Publisher's note: Springer Nature remains neutral with regard to jurisdictional claims in published maps and institutional affiliations.

Methods

Model simulations. In this study, monthly mean outputs from a suite of CMIP5 model simulations are used (see Supplementary Table 1). They include two sets of atmosphere/ocean-coupled experiments for the HIST and RCP8.5 simulations from 37 CMIP5 models, and four sets of fixed-SST atmosphere-only experiments (AMIP, AMIP4×CO_2, AMIP4K and AMIPFuture simulations) from 11 of the 37 CMIP5 models that include outputs of all the selected AMIP-type simulations. For the vertical velocity in HIST and RCP8.5, only 36 out of the 37 models are available; for the energy-related variables in HIST and RCP8.5, only 35 out of the 37 models are available; for the other variables, 37 models are available. See Supplementary Table 1 for the details. The present and future climates are defined as HIST during 1962–2005 and RCP8.5 during 2056–2099, respectively, and the response to global warming is defined as their difference. The standard AMIP simulation is run with observed SSTs and sea-ice and prescribed anthropogenic forcing. In addition to the standard AMIP forcing, three additional AMIP experiments include the quadrupling of CO_2 forcing (AMIP4×CO_2), uniform 4 K SST warming (AMIP4K) and the SST warming pattern from the 1% CO_2 coupled CMIP phase 3 model experiments at the time of CO_2 quadrupling (AMIPFuture). AMIP4×CO_2 – AMIP estimates the climate response to direct radiative forcing, AMIP4K – AMIP estimates the climate response to uniform SST warming and AMIPFuture – AMIP estimates the climate response to the SST warming pattern.

Definitions of atmospheric circulation systems. The Northern Hemispheric subtropical high is defined as the sea-level pressure averaged over 25°–45° N. The Southern Hemispheric subtropical high is defined as the sea-level pressure averaged over 20°–40° S. The Northern Hemispheric mid-latitude westerly is defined as the 925 hPa zonal wind averaged over 40°–55° N. The Southern Hemispheric mid-latitude westerly is defined as the 925 hPa zonal wind averaged over 40°–55° S. Here, we focus on the zonal-mean subtropical highs under global warming. The centre of the Hadley cell is defined as the latitude of zero crossing of the stream function averaged between 400 hPa and 600 hPa between the Northern and Southern Hemispheric cells. The tropical precipitation asymmetry is defined as the zonal-mean precipitation difference between the northern tropics (0°–25° N) and the southern tropics (0°–25° S).

Removing the warmer-get-wetter pattern and wet-get-wetter pattern. To remove the warmer-get-wetter pattern, tropical precipitation change is regressed on the tropical SST change between RCP8.5 and HIST, and the regressed change is removed from the simulated changes. To remove the wet-get-wetter pattern, tropical precipitation change is regressed on the climatological tropical precipitation, and the regressed change is considered as the wet-get-wetter pattern and removed from the simulated changes.

Test of statistical significance. To estimate the statistical robustness of our results, we calculate the number of models with agreement on the sign of the response. As illustrated in a previous study[27], 68% model agreement corresponds to a 95% confidence level. Hence, we use a slightly stricter threshold of 70% model agreement in the whole study to test our results. Our main results are still robust even when we use a stricter threshold of 80% model agreement.

Atmospheric energy analysis. According to the atmospheric energy equation, the divergence of atmospheric energy transport, $\nabla \cdot \mathrm{AHT}$, is equal to the difference between F_{net} and $\frac{\partial <h>}{\partial t}$:

$$\nabla \cdot \mathrm{AHT} = F_{\mathrm{net}} - \frac{\partial <h>}{\partial t} \tag{2}$$

The cross-equatorial energy transport, AHT(0), can be calculated by integrating equation (2) either from the South Pole or from the North Pole to the Equator:

$$\begin{aligned} \mathrm{AHT}(0) &= R^2\left(\int_{-\pi/2}^{0}\int_{0}^{2\pi}\left(F_{\mathrm{net}} - \frac{\partial <h>}{\partial t}\right)\cos\phi \mathrm{d}\lambda \mathrm{d}\phi\right) \\ &= -\int_{0}^{\pi/2}\int_{0}^{2\pi}\left(F_{\mathrm{net}} - \frac{\partial <h>}{\partial t}\right)\cos\phi \mathrm{d}\lambda \mathrm{d}\phi \end{aligned} \tag{3}$$

which can also be written as

$$\begin{aligned} \mathrm{AHT}(0) = \frac{1}{2}R^2\Bigg(&\int_{-\pi/2}^{0}\int_{0}^{2\pi}\left(F_{\mathrm{net}} - \frac{\partial <h>}{\partial t}\right)\cos\phi \mathrm{d}\lambda \mathrm{d}\phi \\ &- \int_{0}^{\pi/2}\int_{0}^{2\pi}\left(F_{\mathrm{net}} - \frac{\partial <h>}{\partial t}\right)\cos\phi \mathrm{d}\lambda \mathrm{d}\phi\Bigg) \end{aligned} \tag{4}$$

where R is the radius of the Earth, ϕ is latitude and λ is longitude. Positive (negative) AHT(0) means northward (southward) cross-equatorial energy transport. In this study, we use equation (4) to calculate the cross-equatorial energy transport.

Relating the latent energy tendency change to the climatological temperature tendency. The latent energy $L_v q$ is closely related to specific humidity, q, which is the product of relative humidity, r, and saturation specific humidity, q_s:

$$L_v q = L_v r q_s \tag{5}$$

The saturation specific humidity, q_s, is a thermodynamic function of pressure, p, and temperature, T. For simplicity, it can be written as

$$q_s = \frac{\epsilon e_s(T)}{p} \tag{6}$$

where e_s is the saturation vapour pressure and ϵ is the ratio of the gas constants for dry air and water vapour. The dependence of e_s on temperature is controlled by the Clausius–Clapeyron equation:

$$\frac{1}{e_s}\frac{\mathrm{d}e_s}{\mathrm{d}T} = \frac{L_v}{R_v T^2} \tag{7}$$

where R_v is the gas constant for water vapour. Equation (7) can be integrated from a reference state that has vapour pressure e_{s0} and temperature T_0 to obtain an explicit relationship between e_s and T:

$$e_s = e_{s0}\mathrm{e}^{\frac{L_v}{R_v}\left(\frac{1}{T_0}-\frac{1}{T}\right)} \tag{8}$$

Combining equations (6) and (8), we can obtain the dependence of the saturation specific humidity q_s on the temperature T:

$$q_s = \frac{\epsilon e_{s0}}{p}\mathrm{e}^{\frac{L_v}{R_v}\left(\frac{1}{T_0}-\frac{1}{T}\right)} \tag{9}$$

At a given pressure level, p, the saturation specific humidity tendency can be obtained by the time, t, derivative of equation (9):

$$\frac{\partial q_s}{\partial t} = \frac{\epsilon L_v e_{s0}}{p R_v T^2}\mathrm{e}^{\frac{L_v}{R_v}\left(\frac{1}{T_0}-\frac{1}{T}\right)}\frac{\partial T}{\partial t} \tag{10}$$

The change of saturation specific humidity tendency between the current and future climatological states (denoted by subscripts c and f, respectively) can be written as

$$\Delta\frac{\partial q_s}{\partial t} = \frac{\epsilon L_v e_{s0}}{p R_v T_f^2}\mathrm{e}^{\frac{L_v}{R_v}\left(\frac{1}{T_0}-\frac{1}{T_f}\right)}\frac{\partial T_f}{\partial t} - \frac{\epsilon L_v e_{s0}}{p R_v T_c^2}\mathrm{e}^{\frac{L_v}{R_v}\left(\frac{1}{T_0}-\frac{1}{T_c}\right)}\frac{\partial T_c}{\partial t} \tag{11}$$

where $T_f = T_c + \Delta T$ and ΔT is the temperature change. Because ΔT is one order of magnitude smaller than T_c, Taylor expansion can be used to simplify equation (11) as

$$\Delta\frac{\partial q_s}{\partial t} \approx \frac{\epsilon L_v e_{s0}\left(\frac{L_v}{R_v}-2T_c\right)}{p R_v T_c^4}\mathrm{e}^{\frac{L_v}{R_v}\left(\frac{1}{T_0}-\frac{1}{T_c}\right)}\Delta T\frac{\partial T_c}{\partial t} \tag{12}$$

Considering that r does not vary greatly at the seasonal cycle and in the future change at the hemispheric scale, we can integrate equation (12) vertically, relate q_s to $L_v q$ using equation (5) and obtain the vertically integrated latent energy tendency change as

$$\Delta\frac{\partial <L_v q>}{\partial t} \approx < \frac{\epsilon L_v^2 r e_{s0}\left(\frac{L_v}{R_v}-2T_c\right)}{p R_v T_c^4}\mathrm{e}^{\frac{L_v}{R_v}\left(\frac{1}{T_0}-\frac{1}{T_c}\right)}\Delta T\frac{\partial T_c}{\partial t} > \tag{13}$$

Because the vertically integrated moisture change is mainly determined by the lower troposphere, ΔT and $\frac{\partial T_c}{\partial t}$ can be estimated by the lower tropospheric or near-surface air temperature, T_s. Therefore, equation (13) can be further simplified as

$$\Delta\frac{\partial <L_v q>}{\partial t} \approx a\Delta T_s\frac{\partial T_s}{\partial t} \tag{14}$$

Here, $a = < \frac{\epsilon L_v^2 r e_{s0}\left(\frac{L_v}{R_v}-2T_c\right)}{p R_v T_c^4}\mathrm{e}^{\frac{L_v}{R_v}\left(\frac{1}{T_0}-\frac{1}{T_c}\right)} >$. Hence, $\Delta\frac{\partial <L_v q>}{\partial t}$ is determined by three factors: the first is a associated with the climatological temperature, the second is ΔT_s and the third is $\frac{\partial T_s}{\partial t}$. On the basis of the simulated values, the seasonal variations of the first two terms are only ~7% of the annual mean in the RCP8.5, AMIP4K and AMIPFuture experiments at the hemispheric scale, so the seasonal variation

of latent energy tendency change is mainly determined by the seasonal variation of the climatological temperature tendency. This is also confirmed in each model and each experiment, as the correlation coefficient between these two variables is nearly 0.90 or higher for the seasonal cycle in each model for the RCP8.5, AMIP4K and AMIPFuture experiments.

Data availability. The data that support the findings of this study are available from the corresponding authors upon request. All data analysed in the study are publicly available. The global climate model outputs can be obtained from the CMIP5 archive, accessed through http://www.ipcc-data.org/sim/gcm_monthly/AR5/Reference-Archive.html.

References

27. Power, S. B., Delage, F., Colman, R. & Moise, A. Consensus on twenty-first-century rainfall projections in climate models more widespread than previously thought. *J. Clim.* **25**, 3792–3809 (2012).